RSC Advances

PAPER

View Article Online
View Journal | View Issue

Cite this: *RSC Adv.*, 2025, **15**, 19468

Ultrasensitive detection of alogliptin *via* fluorescence quenching of terbium-doped carbon quantum dots: mechanistic investigation, Box–Behnken optimization and analytical evaluation†

Ahmed Serag, *[a] Farooq M. Almutairi,[b] Muneef M. Aldhafeeri,[b] Rami M. Alzhrani,[c] Maram H. Abduljabbar,[d] Reem M. Alnemari,[c] Yusuf S. Althobaiti[de] and Atiah H. Almalki[ef]

A rapid, sensitive, and eco-friendly fluorescence-based analytical method was developed for the determination of the antidiabetic drug alogliptin using terbium-doped carbon quantum dots (Tb-CQDs) as a fluorescence probe. The Tb-CQDs were comprehensively characterized using dynamic light scattering, transmission electron microscopy, UV-vis spectroscopy, and fluorescence spectroscopy, revealing uniform spherical nanoparticles with strong blue emission at 448 nm. The sensing mechanism, investigated through Stern–Volmer analysis and thermodynamic studies, demonstrated a static quenching process involving the formation of a ground state complex between Tb-CQDs and alogliptin, with negative ΔH and positive ΔS values confirming the spontaneous interaction driven by hydrogen bonding and van der Waals forces. To maximize analytical performance, critical parameters affecting the quenching process (pH, Tb-CQDs volume, and incubation time) were systematically optimized using a Box–Behnken design of experiments. The statistical analysis through ANOVA confirmed the significance of the obtained quadratic model ($p < 0.0001$), revealing that pH and Tb-CQDs volume significantly influenced quenching efficiency both independently and synergistically. Under optimal conditions (pH 8.8, 1.34 mL Tb-CQDs, 1.2 min incubation), the developed method exhibited excellent linearity in the range of 0.01–1.5 μg mL^{-1} with a limit of detection as low as 3.20 ng mL^{-1}. The validated method was successfully applied for alogliptin analysis in pharmaceutical formulations, spiked human plasma, and environmental water samples, with satisfactory recovery rates (95.10–103.79%). Additionally, the greenness and blueness assessments revealed the superior environmental compatibility and comparable analytical practicality of the Tb-CQDs fluorescence technique compared to conventional HPLC-UV approaches, highlighting the sustainability advantages of this nanomaterial-based sensing platform.

Received 19th April 2025
Accepted 3rd June 2025

DOI: 10.1039/d5ra02737c

rsc.li/rsc-advances

1. Introduction

Fluorescent nanomaterials have gained significant attention in the pharmaceutical and bioanalytical fields due to their unique optical properties, high sensitivity, and selectivity.[1–3] Compared to organic fluorophores, these nanoprobes exhibit enhanced photostability, tunable emission, and the ability to operate in complex matrices.[4] Among the various fluorescent nanomaterials, carbon quantum dots (CQDs) have emerged as promising candidates for sensitive and selective analyte detection owing to their facile synthesis, biocompatibility, and ease of surface functionalization.[5] Their high optical properties could be attributed to the sp^2 and sp^3 hybridized carbon cores with a diverse range of passivating functional groups such as –OH and –COOH.[6] Interestingly, doping these carbon nanoparticles with heteroatoms and metal ions can further improve their fluorescence quantum yield and analyte sensitivity.[7] This enhancement can be attributed to the overlapping atomic orbitals of the heteroatoms and carbon atoms, as well as the push–pull electron action of the heteroatoms.[8] These effects can modify the electronic structure, nanostructure, and chemical

[a]*Pharmaceutical Analytical Chemistry Department, Faculty of Pharmacy, Al-Azhar University, Nasr City 11751, Cairo, Egypt. E-mail: ahmedserag777@hotmail.com*
[b]*Department of Clinical Laboratories Sciences, College of Applied Medical Sciences, University of Hafr AlBatin, Hafr AlBatin 39524, Saudi Arabia*
[c]*Department of Pharmaceutics and Industrial Pharmacy, College of Pharmacy, Taif University, P. O. Box 11099, Taif 21944, Saudi Arabia*
[d]*Department of Pharmacology and Toxicology, College of Pharmacy, Taif University, P. O. Box 11099, Taif 21944, Saudi Arabia*
[e]*Addiction and Neuroscience Research Unit, Health Science Campus, Taif University, P. O. Box 11099, Taif 21944, Saudi Arabia*
[f]*Department of Pharmaceutical Chemistry, College of Pharmacy, Taif University, P. O. Box 11099, Taif 21944, Saudi Arabia*

† Electronic supplementary information (ESI) available. See DOI: https://doi.org/10.1039/d5ra02737c

arrangement of the carbon dots.[8] Among the various dopants, terbium has shown promise due to its ability to effectively sensitize and enhance the fluorescence properties of carbon quantum dots through altering the CQDs' electron density distribution and energy gap thus promoting efficient charge transfer and radiative recombination.[9] Previous comparative studies have demonstrated that terbium doping significantly enhances quantum yields of CQDs, with Chen *et al.* reporting an increase from approximately 12% for undoped CQDs to 32% for terbium doped CQDs (Tb-CQDs).[10] Furthermore, Liu *et al.* demonstrated that terbium-doped CQDs exhibit superior sensing performance with higher sensitivity and selectivity for DNA detection compared to undoped counterparts.[11] Additionally, Xu *et al.* also reported enhanced fluorescence stability and lower detection limits with Tb-doped CQDs for ATP sensing.[12] These collective properties of Tb-CQDs—enhanced quantum yield, improved sensitivity, greater selectivity, and better stability—make them ideal candidates for developing novel analytical methods for pharmaceuticals and environmental pollutants.

Another major advantage in the employing of fluorescent CQDs nanoprobes is its green credential owing to the facile and eco-friendly synthetic approach often involving renewable precursors and mild reaction conditions.[13] The aqueous synthesis of CQDs using organic carbon sources such as citric acid aligns with green chemistry principles by avoiding toxic solvents and harsh reaction conditions, further reducing environmental impact.[14,15] Additionally, the coupled analytical techniques such as UV-vis and spectrofluorimetry are relatively inexpensive, simple to operate, and generate minimal waste, thus rendering the overall method more environmentally benign compared to traditional analytical approaches.[16,17] Multiple toxicological studies have confirmed the significantly lower cytotoxicity and ecotoxicity of carbon-based quantum dots, supporting their classification as environmentally friendly analytical nanoprobes.[18,19] These features highlight the potential of CQDs-based fluorescent assays as a sustainable alternative for pharmaceutical and environmental analysis and aid in promoting the concept of "Green Analytical Chemistry".[20]

Among various pharmaceuticals, alogliptin is an antidiabetic agent belonging to the class of dipeptidyl peptidase-4 inhibitors, which have emerged as a promising treatment strategy for type 2 diabetes mellitus.[21] Diabetes is a chronic metabolic disorder affecting a significant portion of the global population, with substantial morbidity and mortality, necessitating the development of reliable, rapid, and sensitive analytical methods for its management.[22] By inhibiting the DPP-4 enzyme, alogliptin enhances the activity of incretins like glucagon-like peptide-1 and glucose-dependent insulinotropic polypeptide, leading to increased insulin secretion, reduced glucagon release, and improved glycemic control.[23] Given the critical role of alogliptin in diabetes management, it is imperative to establish sensitive, selective, and eco-friendly analytical techniques for its accurate quantification in pharmaceutical formulations as well as in biological and environmental samples.

Literature survey reveals that several analytical techniques, such as reversed phase high-performance liquid chromatography (RP-HPLC),[24–26] liquid chromatography-tandem mass spectrometry (LC-MS/MS),[27,28] and spectrophotometry,[29] have been employed for the determination of alogliptin. However, these methods often suffer from drawbacks like complex sample preparation, high operational cost, and the use of hazardous organic solvents. Spectrophotometric methods, on the other hand, are limited by poor sensitivity and selectivity. A recent study employed screen-printed potentiometric sensor for alogliptin determination, but the technique required electrode fabrication and suffer from poor sensitivity.[30] The only reported fluorescence-based methods for alogliptin detection utilized derivatization with fluorescent tags such as 4-chloro-7-nitrobenzofurazan (NBD-Cl),[31] fluoroscamin[32] and ninhydrin[33] which suffer from tedious derivatization steps and the use of toxic reagents.

Therefore, the present study aims to establish the first fluorescence-based analytical approach for alogliptin determination using an eco-friendly, sensitive, and selective Tb-CQDS nanoprobe as a "turn-off" fluorescent probe, which can serve as a sustainable alternative to conventional analytical techniques. The key objectives include: (1) synthesis and comprehensive characterization of Tb-CQDS nanoprobe using various techniques and investigation of their optical properties using UV-vis and spectrofluorimetric analysis. (2) Investigation of the sensing mechanism between Tb-CQDS and alogliptin through Stern–Volmer quenching analysis and thermodynamic studies. (3) Optimization of factors affecting the experimental conditions, such as pH, Tb-CQDS volume, and incubation time, using a Box–Behnken experimental design to gain maximum analytical sensitivity and robustness. (4) Validation of the analytical performance according to ICH guidelines in terms of linearity, sensitivity, accuracy, precision, robustness, and selectivity. (5) Demonstration of the practical applicability by analyzing alogliptin in pharmaceutical formulations, spiked human plasma, and environmental water samples (river and tap water). (6) Assessment of the greenness and blueness of the developed method using AGREE[34] and BAGI[35] tools to evaluate its environmental impact and analytical practicality in comparison with reported literature.

2. Experimental

2.1. Materials and reagents

Alogliptin benzoate (99.8% purity) was obtained from the Egyptian Drug Authority in Cairo, Egypt. Terbium(III) nitrate pentahydrate $Tb(NO_3)_3 \cdot 5H_2O$, HPLC grade solvents including ethanol and acetonitrile were sourced from Sigma-Aldrich (St. Louis, Missouri, USA). Analytical grade reagents including acetic acid, sodium hydroxide, phosphoric acid, boric acid, citric acid, and sodium chloride were obtained from Piochem Co., Cairo, Egypt. Distilled water was used throughout the study. The pharmaceutical dosage form Deltaglipt® containing 25 mg alogliptin per tablet was purchased from a local pharmacy in Cairo, Egypt. Human plasma samples were purchased from VACSERA CO., Giza, Egypt and stored at −20 °C until analysis.

Britton–Robinson buffer solutions (BR, pH 5–10) were prepared by mixing 0.04 M phosphoric acid, 0.04 M boric acid, and 0.04 M acetic acid, and adjusting the pH using 0.2 M sodium hydroxide.

2.2. Instrumentation

UV-vis absorption spectra were recorded on a Shimadzu UV-1800 spectrophotometer operated in the wavelength range of 200–500 nm using 1 cm quartz cuvettes. Fluorescence measurements were performed on a Jasco FP-8300 spectrofluorometer equipped with a 150 W xenon lamp and a 1 cm quartz cell. The instrumental parameters were set with excitation and emission slit widths of 10 nm and a scan rate of 4000 nm min^{-1}. Particle size distribution analysis was conducted using a Malvern ZEN3600 Zetasizer Nano ZS instrument, while transmission electron microscopy was carried out using a JEM-2100F microscope operated at an accelerating voltage of 200 kV. pH measurement was performed using a Jenway 3510 pH meter equipped with a glass electrode. The pK_a values and ionization states of alogliptin were calculated using MarvinSketch (version 24.3.2, Chemaxon), (**https://www.chemaxon.com**).

2.3. Synthesis and characterization of Tb-CQDs

Tb-CQDs were synthesized *via* a one-pot carbonization method adapted from Chen *et al.* with slight modifications.[10] Terbium nitrate pentahydrate (0.5 g) and citric acid (1 g) were mixed in a bottom round-bottomed flask at a molar ratio of 1 : 4.5. The mixture was heated in a thermostatic oil bath at 190 °C for 1 hour. After cooling down to room temperature, the resulting carbonization products were dissolved in 10 mL of distilled water, filtered through a 0.45 μm membrane, and the resulting solution of Tb-CQDs was obtained as a yellow liquid. The obtained Tb-CQDs were precipitated by 95% ethanol and washed with ethanol several times to remove any unreacted precursors, then dried in a vacuum oven at 50 °C. A stock solution of Tb-CQDs was prepared in distilled water at a concentration of 1 mg mL^{-1} (approximately 36.6 μM, calculated based on the average particle diameter of 3.71 nm and estimated molar mass of 27 300 g mol^{-1}) and used for further studies. The quantum yield of the synthesized Tb-CQDs was determined to be 37% using quinine sulfate in 0.1 M H_2SO_4 (quantum yield = 54%) as a reference standard following the IUPAC method described by Brouwer.[36] The synthesized Tb-CQDs were extensively characterized *via* dynamic light scattering (DLS), transmission electron microscopy (TEM), UV-vis absorption, and spectrofluorimetry to investigate their size, morphology, optical properties, and fluorescence behavior using standard analytical protocols.

2.4. Optimization of the sensing conditions

A Box–Behnken experimental design was employed to optimize the analytical conditions for alogliptin sensing using Tb-CQDs. The independent variables included the Britton–Robinson buffer pH (5–10), Tb-CQDs volume (0.5–1.5 mL) of 1 mg per mL stock solution, corresponding to final concentrations of approximately 1.83–5.49 μM, and incubation time (1–5 min). Each variable was studied at three levels: low, medium, and high, resulting in 17 experimental runs. The Box–Behnken design was chosen over other response surface designs due to its rotatable quadratic design properties and efficiency in exploring the design space with fewer experimental runs as described by Ferreira *et al.*[37] The quenching efficiency percentage (QE%) was evaluated as the response variable using the equation:

$$\text{Quenching efficiency}\% = (F_0 - F)/F_0 \times 100 \quad (1)$$

where F_0 and F are the fluorescence intensities of Tb-CQDS in the absence and presence of alogliptin, respectively. The optimized conditions were determined by the desirability function to obtain maximum quenching efficiency using Design-Expert software (version 11.1.2.0) for maximum sensing of alogliptin.

2.5. Construction of the fluorescent nanoprobe

In a series of 10 mL volumetric flasks, different volumes of alogliptin working solutions were added, followed by 1.34 mL of Tb-CQDs stock solution (1 mg mL^{-1}, resulting in a final concentration of approximately 4.91 μM) and 1 mL of BR-buffer solution (pH 8.8). The resulting mixtures were shaken and allowed to incubate for 1.2 minutes, with the volume made up to the mark with distilled water. The fluorescence intensity of each solution was measured at excitation and emission wavelengths of 334 nm and 448 nm, respectively, against a blank solution containing all reagents except alogliptin. For each measurement, the exact same fluorescence acquisition parameters were maintained, including excitation/emission slit widths (10 nm), and scan speed (4000 nm min^{-1}). The quenching of Tb-CQDs fluorescence intensity by alogliptin (F_0/F) was plotted to construct the calibration curve.

2.6. Method validation

The developed fluorescence-based detection method for alogliptin was validated according to the ICH Q2(R1) guidelines to evaluate its linearity, sensitivity, accuracy, precision, robustness, and selectivity.

Linearity was assessed by constructing calibration curves in the concentration range of 0.01 to 1.5 μg per mL alogliptin. The regression equation and correlation coefficient (r^2) were determined. Limits of detection and quantification were calculated based on the standard deviation of the blank and the slope of the calibration curve. Ten replicate measurements of blank solutions (containing all reagents except alogliptin) were performed under identical conditions, and the standard deviation (σ) of these measurements was calculated. The LOD and LOQ were then calculated using the following equations:

$$\text{LOD} = 3.3\sigma/S \quad (2)$$

$$\text{LOQ} = 10\sigma/S \quad (3)$$

where S is the slope of the calibration curve.

Accuracy was evaluated by the recovery study using three concentration levels (0.02, 0.75, and 1.2 μg mL^{-1}) in triplicate.

Repeatability and intermediate precision were determined by analyzing the same samples under the same conditions on the same day and on different days, respectively. Robustness was investigated by evaluating the influence of small variations in experimental conditions like pH, and Tb-CQDs volume on the assay performance. The selectivity of the method was assessed by investigating the potential interference from various excipients and common ions that may be present in pharmaceutical formulations and environmental samples at 10-fold excess. Additionally, common components of plasma samples such as tryptophan, tyrosine, glutamic acid, glucose and albumin were examined for their impact on the method selectivity.

2.7. Application to real samples

The proposed Tb-CQDs fluorescence method was successfully applied for the determination of alogliptin in commercial tablet dosage form, spiked human plasma samples, and environmental water samples including river and tap water. For the tablet analysis, ten tablets were weighed, powdered and an amount of 10 mg equivalent to alogliptin was accurately weighed, dissolved in 50 mL distilled water and sonicated for 20 minutes. The solution was then filtered through a 0.45 μm membrane filter and diluted to 100 mL with distilled water. Working solutions were prepared through sequential dilution of this stock solution, which were then analyzed using the developed fluorescence-based method.

The proposed Tb-CQDs fluorescence method was also applied for alogliptin determination in spiked human plasma samples. Four plasma sample sets were prepared by spiking 1 mL of fresh human plasma with alogliptin to achieve initial concentrations of 1, 7.5, 10, and 12.5 μg mL^{-1}, corresponding to final concentrations of 0.1, 0.75, 1, and 1.25 μg mL^{-1} after method application. Each spiked plasma sample underwent deproteinization by adding an equal volume of acetonitrile and centrifuging at 4000 rpm for 10 minutes. The resulting supernatant was collected and dried under a gentle nitrogen stream at 40 °C. The dried residue was then directly reconstituted in 1.34 mL of Tb-CQDs stock solution and 1 mL of Britton–Robinson buffer (pH 8.8) and diluted to 10 mL with distilled water. The fluorescence intensity was measured at excitation and emission wavelengths of 334 nm and 448 nm, respectively, against a blank solution prepared using the same procedure.

Environmental water samples, including river and tap water, were analyzed using a similar approach. Water samples were first filtered through a 0.45 μm membrane filter to remove suspended particles. Four sets of reiver and tap water samples were spiked to achieve initial alogliptin concentrations of 1, 7.5, 10, and 12.5 μg mL^{-1}, which correspond to final concentrations of 0.1, 0.75, 1, and 1.25 μg mL^{-1} after method application. The analysis procedure mirrored the plasma sample protocol: 1 mL of spiked water was combined with 1 mL of acetonitrile and 250 mg NaCl to allow phase separation followed by centrifugation at 4000 rpm for 10 minutes. The supernatant was collected, dried under nitrogen, and reconstituted with 1.34 mL of Tb-CQDs stock solution, 1 mL of Britton–Robinson buffer (pH 8.8), then diluted to 10 mL with distilled water. Fluorescence measurements were conducted using optimized spectrofluorimetric conditions. Each sample type was analyzed in triplicate to ensure statistical reliability.

3. Results and discussion

3.1. Characterization and optical properties of Tb-CQDs

The synthesized Tb-CQDs were thoroughly characterized to understand their physicochemical properties and optical behavior. Dynamic light scattering (DLS) analysis revealed an average hydrodynamic diameter of 3.71 ± 0.9 nm for the Tb-CQDs (Fig. 1A). This relatively monodisperse size distribution is a desirable attribute, as it ensures consistent and uniform optical and sensing performance of the nanomaterial. The small size of the Tb-CQDs also indicates a high surface-to-volume ratio, which can enhance their interaction with target analytes and improve detection sensitivity. Transmission electron microscopy (TEM) further corroborated the DLS findings, clearly showing the Tb-CQDs had a uniform spherical morphology (Fig. 1B). The spherical shape and nanoscale dimensions of the Tb-CQDs are advantageous, as they can facilitate efficient surface functionalization, improved dispersibility, and enhanced fluorescence properties compared to larger or irregular-shaped carbon-based nanomaterials.

The UV-vis absorption spectrum of the Tb-CQDs exhibited a distinct peak at 338 nm (Fig. 1C), which can be attributed to the n–π* transitions of the carbonyl groups on the CQD surface. This absorption characteristic is a common feature of carbon quantum dots and indicates the successful incorporation of functional groups during the synthetic process. These surface moieties not only contribute to the optical properties but also provide sites for potential analyte interactions and further surface modifications. Importantly, the Tb-CQDs displayed strong fluorescence emission centered at 448 nm upon excitation at 334 nm (Fig. 1D). The measured fluorescence quantum yield of 37% using quinine sulfate method is particularly noteworthy, as it demonstrates the efficient sensitization of terbium ions by carbon dots. The observed blue emission and high quantum yield of the Tb-CQDs can be attributed to the effective overlap of atomic orbitals between the terbium dopant and the carbon core, as well as the push–pull electron interactions facilitated by the terbium ions. The photostability of the synthesized Tb-CQDs was also evaluated as an important property for reliable analytical applications. When subjected to continuous excitation at 334 nm over a 3-hour period, the Tb-CQDs maintained approximately 94.2% of their original emission intensity, demonstrating excellent resistance to photobleaching (Fig. S1†). These unique optical properties of the Tb-CQDs make them well-suited as fluorescent probes for the selective and sensitive detection of alogliptin in this study.

3.2. Mechanism of alogliptin detection by Tb-CQDs

Upon investigating the fluorescence response of Tb-CQDs towards alogliptin, a significant fluorescence quenching effect was observed (Fig. 2A). This quenching phenomenon can be attributed to various mechanisms such as (i) static quenching

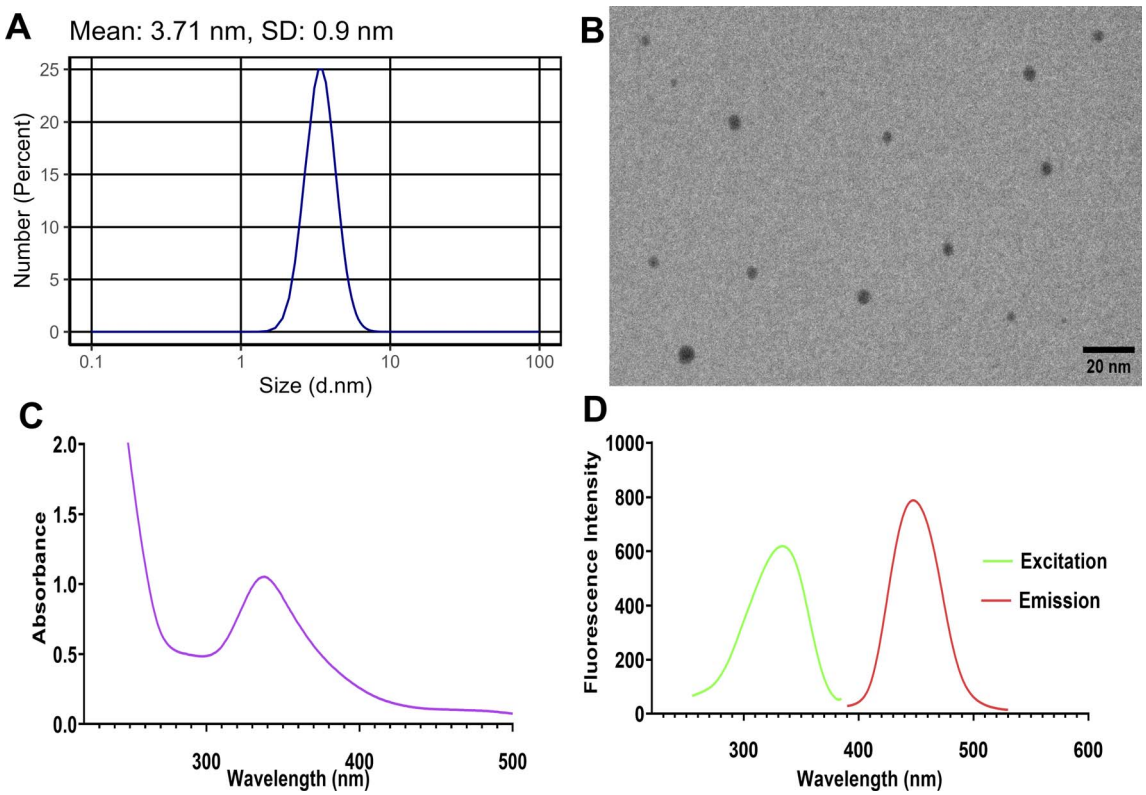

Fig. 1 Characterization of Tb-CQDs: (A) DLS size distribution of synthesized Tb-CQDs, (B) TEM micrograph showing uniform spherical morphology (scale bar = 20 nm), (C) UV-vis absorption spectrum of Tb-CQDs with a distinct peak at 338 nm, and (D) fluorescence spectra with maximum excitation at 334 nm and maximum emission at 448 nm.

due to the formation of a non-fluorescent ground-state complex between alogliptin and Tb-CQDs, (ii) dynamic quenching resulting from collisional encounters between the excited Tb-CQDs and alogliptin, and (iii) energy transfer from the excited Tb-CQDs to alogliptin. Hence, temperature dependent fluorescence studies were conducted to elucidate the predominant quenching mechanism using Stern–Volmer analysis (Fig. 2B):

$$F_0/F = 1 + K_{sv}[Q] \quad (4)$$

where F_0 and F are the fluorescence intensities of Tb-CQDs in the absence and presence of alogliptin, respectively, and K_{sv} is the Stern–Volmer quenching constant. The linear Stern–Volmer plots obtained at different temperatures (298, 303, and 313 K) revealed that the K_{sv} decreased from 9.44×10^5 M^{-1} at 298 K to 6.73×10^5 M^{-1} at 313 K, as shown in Table 1. This observed decrease in the K_{sv} values with increasing temperature suggests a static quenching mechanism, where a non-fluorescent ground-state complex is formed between alogliptin and Tb-CQDs. This was further corroborated by calculating the bimolecular quenching rate constant (K_q) using the equation:

$$K_q = K_{sv}/\tau_0 \quad (5)$$

where K_q is the bimolecular quenching rate constant, τ_0 is the lifetime of Tb-CQDs in the absence of alogliptin which is reported to be 3.98 ns.[10] The resulting K_q value was on the order of 10^{14} M^{-1} s^{-1}, substantially exceeding the diffusion-controlled limit (2×10^{10} M^{-1} s^{-1}), confirming the static quenching nature of the interaction between Tb-CQDs and alogliptin.

The association constant (K_a) was also calculated using the modified Stern–Volmer equation:

$$F_0/(F_0 - F) = 1 + 1/(K_a[Q]) \quad (6)$$

The obtained K_a values also decreased from 1.49×10^6 M^{-1} at 298 K to 9.4×10^5 M^{-1} at 313 K (Table 1), further confirming the static quenching nature of the interaction (Fig. 2C). The high association constant values (K_a) observed in this study indicate strong binding affinity between Tb-CQDs and alogliptin. These values are consistent with the formation of a stable ground-state complex, which is characteristic of static quenching processes. The decrease in K_a values with increasing temperature further supports this conclusion, as higher temperatures typically destabilize ground-state complexes.

The thermodynamic parameters, including Gibbs free energy (ΔG), enthalpy (ΔH), and entropy (ΔS) changes, were calculated using the van't Hoff equation (Fig. 2D). The negative value of ΔH (-23.59 kJ mol^{-1}) and the positive value of ΔS (39.02 J (mol^{-1} K^{-1})) indicated that the interaction between Tb-CQDs and alogliptin was spontaneous and driven by both hydrogen bonding and van der Waals forces (Table 1). The increase in system entropy suggests that the binding process is accompanied by the release of water molecules from the

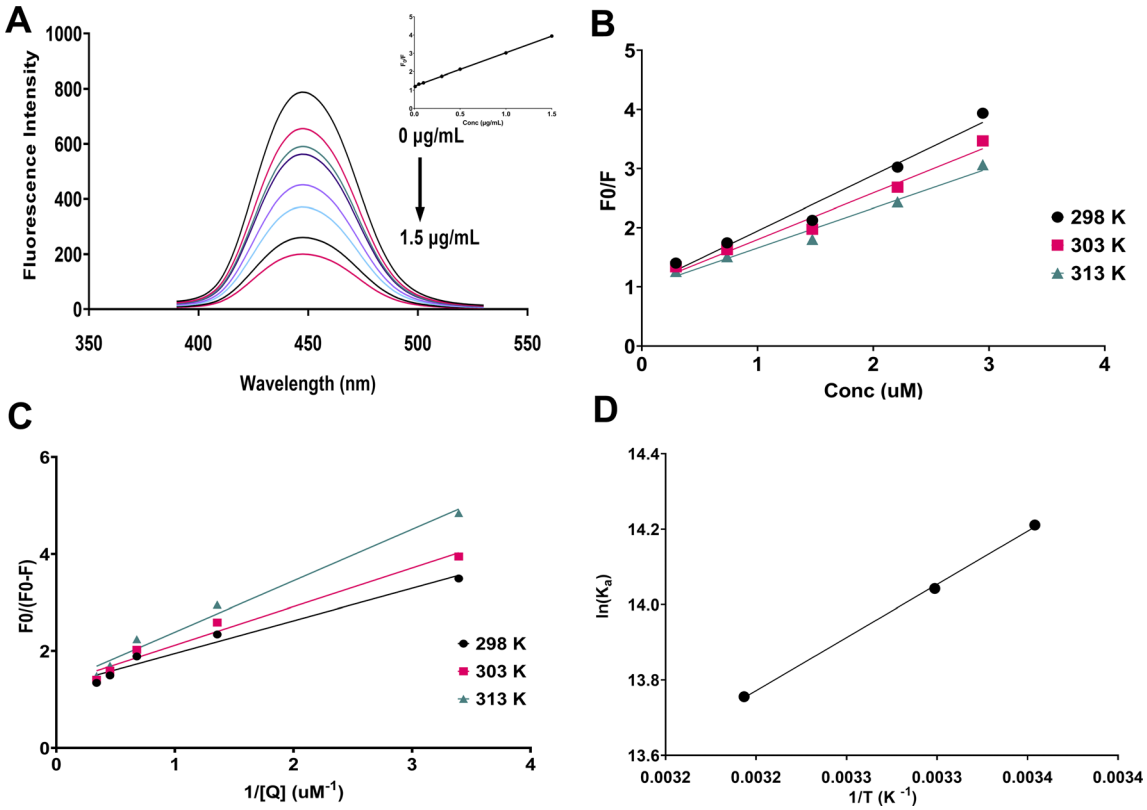

Fig. 2 Mechanistic investigation of alogliptin detection by Tb-CQDs: (A) fluorescence quenching of Tb-CQDs in the presence of different alogliptin concentrations; the inset shows linear relation between the quenching ratio (F_0/F) and alogliptin concentrations. (B) Stern–Volmer plots for static quenching at different temperatures (298 K, 303 K, and 313 K), (C) modified Stern–Volmer plots for static quenching at different temperatures (298 K, 303 K, and 313 K) used to determine the association constant (K_a), and (D) van't Hoff plot for thermodynamic analysis of the Tb-CQDs and alogliptin interaction.

hydration shell of the interacting species, leading to an increase in the overall randomness of the system. The negative value of ΔG (-35.23 kJ mol^{-1}) confirmed the favorable and spontaneous nature of the binding process.

It is worth noting that fluorescence lifetime measurements would provide additional insights into the quenching mechanism. In static quenching, the formation of a non-fluorescent ground-state complex would not affect the fluorescence lifetime of the remaining fluorophores, while dynamic quenching would lead to a reduction in fluorescence lifetime proportional to the quencher concentration. While such measurements were beyond the scope of the current study, the observed temperature dependence of K_{sv} values strongly supports a static quenching mechanism, as higher temperatures typically destabilize ground-state complexes, resulting in decreased quenching efficiency. This temperature effect, combined with the thermodynamic parameters and calculated quenching rate constants that exceed the diffusion limit, provides compelling evidence for a static quenching process in the Tb-CQDs-alogliptin system. At the optimized pH, the Tb-CQDs surface is predominantly negatively charged due to deprotonation of carboxyl groups (p$K_a \sim 4.5$), while alogliptin (p$K_a \sim 9.4$) exists partially in its protonated form. Favorable electrostatic interactions are created between the negatively charged Tb-CQD surface and the partially positively charged nitrogen in alogliptin's piperidine ring. Additionally, the negative ΔH value (-23.59 kJ mol^{-1}) and positive ΔS value (39.02 J (mol^{-1} K^{-1})) suggest that hydrogen bonding plays a significant role, likely occurring between the hydroxyl and carbonyl groups on the Tb-CQD surface and the amide and uracil moieties of alogliptin. The significantly negative ΔG values (ranging from -35.23 to -35.81 kJ mol^{-1} across the tested temperature range) confirm

Table 1 Stern–Volmer and thermodynamic parameters for the interaction between Tb-CQDs and alogliptin at different temperatures

Temperature (K)	K_{sv} (10^5 M^{-1})	K_a (10^6 M^{-1})	ΔG (kJ mol^{-1})	ΔH (kJ mol^{-1})	ΔS (J (mol^{-1} K^{-1}))
298	9.44	1.49	−35.23	−23.59	39.02
303	7.90	1.25	−35.39		
313	6.73	0.94	−35.81		

the favorable and spontaneous nature of the binding process. The ground-state complex formation leads to efficient fluorescence quenching, and this proposed mechanism is consistent with all experimental observations and explains the high sensitivity and selectivity of the sensing platform for alogliptin detection. Based on these mechanistic insights, factors affecting the binding equilibrium, such as pH and Tb-CQDs concentration, were identified as critical parameters to be optimized for maximizing analytical performance. Consequently, a Box–Behnken design was employed to systematically optimize these parameters and develop a robust analytical method.

3.3. Optimization of detection conditions

The quenching efficiency of Tb-CQDs towards alogliptin was further optimized by evaluating the influence of various experimental parameters, including solution pH, Tb-CQDs volume, and incubation time, using a Box–Behnken experimental design. Apparently, pH is one of the most critical factors, as it can significantly affect the fluorescence properties of Tb-CQDs as well as the ionization state of alogliptin. The pK_a of alogliptin is around 9.4, and it exists in both cationic and neutral forms depending on the pH of the solution (Fig. S2A†). At lower pH values, the cationic form of alogliptin can interact more strongly with the negatively charged Tb-CQDs leading to enhanced quenching due to more favorable electrostatic interactions between the positively charged alogliptin and the negatively charged Tb-CQDs surface at this pH range. Particularly, the amino group of alogliptin get protonate at pH values below 9.4, which facilitates the complexation with Tb-CQDs and results in higher quenching efficiency, as shown in (Fig. S2B†). However, a compromise must be made between the quenching efficiency and the stability of the Tb-CQDs, as excessively low pH values can deteriorate the fluorescence properties of the nanoprobe. Hence, pH in the range of 5–10 was employed for further optimization. The volume of Tb-CQDs is another crucial parameter, as it determines the concentration of the fluorescent probe available for interaction with alogliptin. Also, the incubation time is important as it allows the system to reach equilibrium for effective complexation between Tb-CQDs and alogliptin. Hence, the effects of these three parameters (pH, Tb-CQDs volume, and incubation time) were optimized using a Box–Behnken design, and the results are fitted to a quadratic model followed by backward elimination:

$$\mathrm{QE\%} = 55.9882 + 9.82274A + 10.4272B + 7.70813AB - 14.1863A^2 - 10.5944B^2 \quad (7)$$

where A is the pH, B is the Tb-CQDs volume, and the response (QE%) is the quenching efficiency. ANOVA analysis of this reduced quadratic model reveal a significant model with $F = 22.79$ and $p < 0.0001$, indicating the model's adequacy in predicting the quenching efficiency. Moreover, the lack-of-fit test showed a non-significant value ($p = 0.98$), confirming the good fit of the model (Table S1†). In terms of individual factors, both the main parameters (pH and Tb-CQDs volume), their interaction and quadratic terms exhibited a significant effect on the quenching efficiency ($p < 0.05$). The sign of the coefficients suggested that an increase in pH and Tb-CQDs volume would result in enhanced quenching up to an optimum level, beyond which the response would decrease. This quadratic model provides valuable analytical information beyond identifying optimal conditions. The synergistic interaction between pH and Tb-CQDs volume (positive AB coefficient) offers mechanistic insight into the sensing system, confirming that the ionization states of both the analyte and nanoprobe cooperatively enhance complex formation. The negative quadratic terms (A^2 and B^2) define a region of analytical robustness around the optimum conditions, within which small variations in experimental parameters would minimally affect method performance – a critical consideration for routine analytical applications in complex matrices.

This comes in line with the plots of each parameter and their combined effect on the quenching efficiency (Fig. 3). A curvature can be observed in the pH indicating the presence of an optimum region (Fig. 3A). This could be attributed to the pH-dependent fluorescence characteristics of Tb-CQDs as previously discussed, with ideal quenching occurring at slightly basic conditions due to the protonation of alogliptin and the deprotonation of Tb-CQDs making the formation of the ground state complex more favorable. Similarly, the increasing trend of quenching efficiency with Tb-CQDs volume leveled off at higher volumes (Fig. 3B), indicating that a maximum amount of the fluorescent probe has been reached for optimal interaction with alogliptin. The decrease in quenching efficiency at higher Tb-CQDs concentrations could be due to various factors such as self-quenching and aggregation of the Tb-CQDs. The incubation time had no effect as evident from the non-significant coefficient and the straight horizontal line (Fig. 3C), indicating that the system reached equilibrium very fast. The interaction between pH and Tb-CQDs volume showed a positive effect, implying that the two factors work synergistically to enhance the quenching process as evident from the 3D-response surface plot further support the findings of the model (Fig. 3D).

Validity tests of the model were conducted, including inspecting the fit statistics, residual plots, and the predicted *vs.* actual response. The model exhibited an excellent fit with high R^2 (0.9120), adjusted R^2 (0.8720), predicted R^2 (0.8550), and adequate precision (12.71), confirming the adequacy of the model in describing the experimental data. The normal probability plot of the residuals and the predicted *vs.* actual plot both show linear trends (Fig. S3†), validating the assumptions of the model. The effect of run order was also non-significant, demonstrating the robustness of the experimental design (Fig. S4†). Desirability function analysis was employed to determine the optimal conditions for the quenching process, aiming to maximize the quenching efficiency. The systematic optimization using Box–Behnken design successfully identified the optimal conditions for maximum quenching efficiency of Tb-CQDs by alogliptin: pH 8.8, Tb-CQDs volume of 1.34 mL (corresponding to a final concentration of 4.91 μM), and incubation time of 1.2 min. Under these optimized conditions, a quenching efficiency of 62.18% was achieved (Fig. 4).

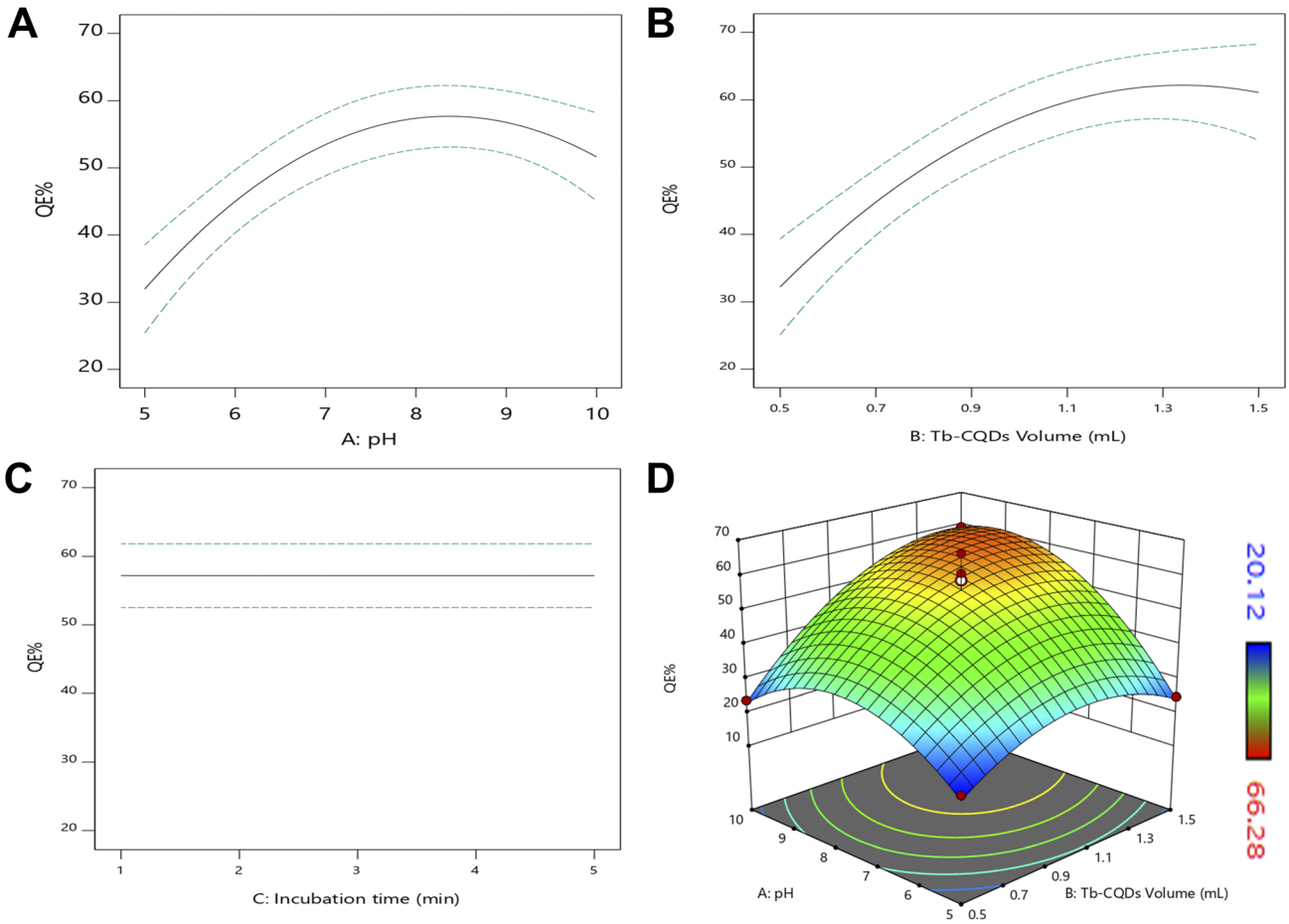

Fig. 3 Box–Behnken optimization plots depicting the influence of (A) pH, (B) Tb-CQDs volume, and (C) incubation time on quenching efficiency. (D) 3D surface response plot, highlighting the combined effects of pH and Tb-CQDs volume on the fluorescence quenching response.

In addition to pH, Tb-CQDs volume, and incubation time, the effect of ionic strength on the quenching efficiency was also investigated as an important parameter that could affect the analytical performance. The quenching efficiency was measured at different NaCl concentrations (0–500 mM) while maintaining other optimized conditions (pH 8.8, Tb-CQDs volume 1.34 mL, incubation time 1.2 min). As shown in Fig. S5,† the quenching efficiency remained remarkably stable at low to moderate ionic strength (0–100 mM NaCl), with minimal variation (<3%). However, as the ionic strength increased beyond 100 mM NaCl, a pronounced decrease in quenching efficiency was observed, with approximately 30% reduction at 300 mM NaCl and 49% reduction at 500 mM NaCl compared to the no-salt condition. This negative effect of high ionic strength on quenching efficiency can be attributed to the screening of electrostatic interactions between the negatively charged Tb-CQDs surface and the partially positively charged alogliptin at the working pH. Higher ionic strength shields these attractive forces, reducing complex formation. Based on these findings, all subsequent experiments were conducted without additional salt to maintain maximum sensitivity, although the method demonstrates excellent stability within the ionic strength range of 0–100 mM NaCl, which covers most biological and environmental samples after routine sample preparation.

Hence, these optimized conditions were subsequently utilized to develop and validate an analytical method for alogliptin determination according to ICH guidelines. The validation studies aimed to evaluate the critical analytical performance characteristics, including linearity, sensitivity, accuracy, precision, robustness, and selectivity, to establish the reliability and applicability of the proposed method in various sample matrices.

3.4. Validation of the developed method

The developed Tb-CQDs based "on–off" fluorescence method for the determination of alogliptin was validated according to the ICH guidelines in terms of linearity, sensitivity, accuracy, precision, robustness, and selectivity (Table 2). Linearity was evaluated by constructing calibration curves in the concentration range of 0.01–1.5 μg mL^{-1}, exhibiting excellent linear correlation (r^2 > 0.9990) within this range. The regression equation was found to be:

$$Y = 1.8142C + 1.2131 \quad (8)$$

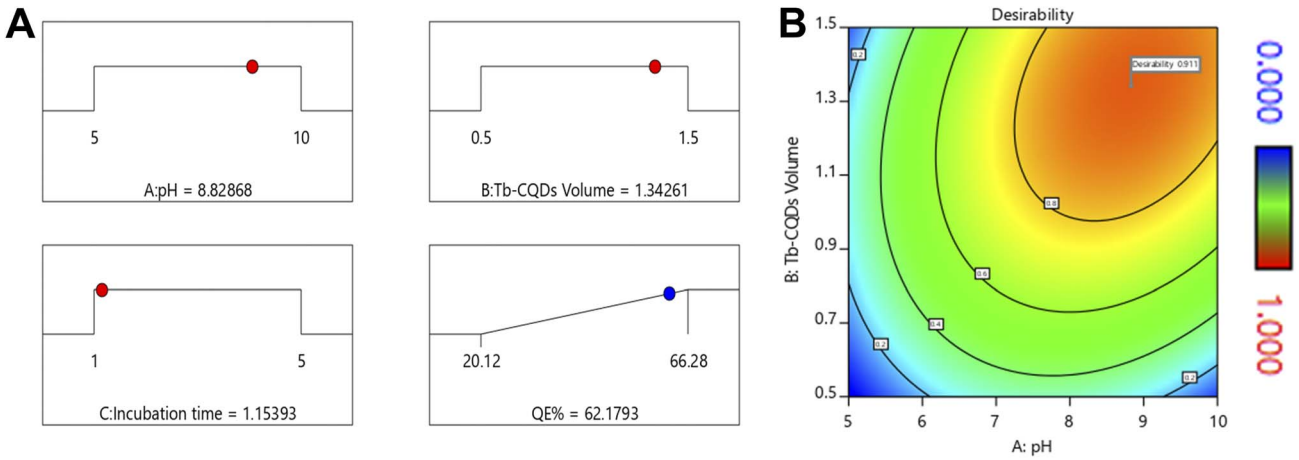

Fig. 4 Desirability function analysis for the optimization of detection conditions. (A) Individual conditions for pH, Tb-CQDs volume, and incubation time that achieve the maximum quenching efficiency. (B) Overall desirability contour plot showing the combined effect of pH and Tb-CQDs volume on the quenching efficiency.

Table 2 Validation parameters for the developed fluorescence-based method for alogliptin determination according to ICH guidelines

Parameters		Alogliptin
Excitation wavelength (nm)		334
Emission wavelength (nm)		448
Linearity range (μg mL^{-1})		0.01–1.5
Slope		1.8142
Intercept		1.2131
Correlation coefficient (r^2)		0.9997
LOD (μg mL^{-1})		0.0032
LOQ (μg mL^{-1})		0.0096
Accuracy (% R)[a]		98.64 ± 1.21
Repeatability precision (% RSD)[b]		1.227
Intermediate precision (% RSD)[c]		1.715
Robustness (% R)	Buffer (pH)	99.44 ± 1.117
	Tb-CQDs (mL)	98.30 ± 0.701

[a] Average of 9 determinations (3 concentrations repeated 3 times). [b] % RSD of 9 determinations (3 concentrations repeated 3 times) measured on the same day. [c] % RSD of 9 determinations (3 concentrations repeated 3 times) measured in the three consecutive days.

where Y is the fluorescence response (F_0/F) and C is the concentration of alogliptin in μg mL^{-1}, with a coefficient of determination (r^2) of 0.9997. The limits of detection and quantification were determined to be 3.20 ng mL^{-1} and 9.60 ng mL^{-1}, respectively, indicating the high sensitivity of the proposed method. Compared to the gold standard HPLC-UV method,[24] the present Tb-CQDs based fluorescence sensor showed significantly lower LOD (3.20 ng mL^{-1} *vs.* 8.32 ng mL^{-1}) and LOQ (9.60 ng mL^{-1} *vs.* 24.96 ng mL^{-1}).

Accuracy was evaluated through recovery experiments at three concentration levels in triplicates, yielding average recoveries 98.64 ± 1.21%, demonstrating the accuracy of the method. Precision was assessed in terms of both repeatability and intermediate precision, with % RSD values less than 2% in all cases, confirming the high precision of the method (Table 2). Robustness of the method was evaluated by introducing small deliberate changes in the optimized conditions such as pH (±0.1) and Tb-CQDs volume (±0.1 mL), which resulted in minimal variations, confirming the robustness of the developed method (Table 2).

The selectivity was extensively validated against a variety of potential interferences, including pharmaceutical excipients (*e.g.*, starch, lactose, magnesium stearate, and cellulose) and environmental ions (*e.g.*, Na^+, K^+, Ca^{2+}, Mg^{2+}, Ni^{2+}, Cd^{2+}, SO_4^{2-}, and PO_4^{3-}). None of these significantly influenced the fluorescence signal (Fig. 5). Similarly, negligible quenching effects were observed with common plasma components such as glucose, albumin, and amino acids, as well as pooled plasma samples (Fig. 5). These findings confirm the method's high

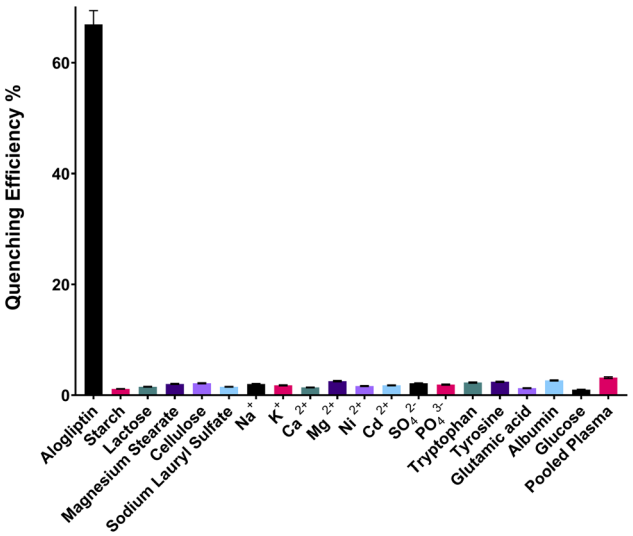

Fig. 5 Selectivity of the Tb-CQDs-based fluorescent probe for alogliptin detection: Evaluation of quenching efficiency in the presence of potential interferents (at 10-fold excess, 10 μg mL^{-1}) relative to alogliptin (1 μg mL^{-1}), including pharmaceutical excipients, common ions, plasma components, and pooled plasma. Error bars represent standard deviation of triplicate measurements (n = 3).

selectivity for alogliptin in pharmaceutical formulations, environmental and biological matrices.

3.5. Application to pharmaceutical, biological, and environmental samples

Following the comprehensive validation of the method according to ICH guidelines, which established its reliability and analytical performance characteristics, the practical applicability of the developed Tb-CQDs fluorescence method was demonstrated by analyzing alogliptin in diverse real-world samples. While method validation focused on evaluating the analytical performance parameters, this application study aimed to evaluate the method's effectiveness in dealing with various sample matrices of pharmaceutical, biological, and environmental origin. Consequently, the validated Tb-CQDs-based fluorescence method was applied for the quantitative determination of alogliptin in pharmaceutical dosage forms, spiked human plasma, and environmental water samples (river and tap water).

For the analysis of pharmaceutical formulations, the proposed method demonstrated excellent recovery, with a mean value of 99.87 ± 1.27% relative to the labeled claim (Table 3). This finding confirms the applicability of the developed technique for the routine quality control analysis of alogliptin in commercial drug products. Statistical comparison of the results obtained by the proposed Tb-CQDs fluorescence method and a reported HPLC-UV method[24] revealed no significant differences (Table 3). The Student's *t*-test yielded a calculated *t*-value of 0.218, which was well below the critical *t*-value of 2.306 at a 95% confidence level. This indicates that the accuracy of the developed method is statistically comparable to the established HPLC-UV method. Furthermore, the *F*-test for variance comparison produced an *F*-value of 5.547, which was also lower than the critical *F*-value of 6.338, further confirming the precision and reliability of the Tb-CQDs fluorescence approach. Interval hypothesis testing was employed to evaluate the 95% confidence interval of the mean recovery. The lower and upper bounds of the confidence interval were determined to be $\theta_L = -1.292\%$ and $\theta_U = 1.562\%$, respectively. These results demonstrate that the method's accuracy falls well within the acceptable bias range of ±2%, reinforcing the suitability of the Tb-CQDs fluorescence technique for the quantitative determination of alogliptin in pharmaceutical formulations.

The developed Tb-CQDs fluorescence-based analytical method was further validated through extensive recovery studies using spiked human plasma samples (Table 4). The recoveries obtained were in the range of 97.07–103.72%, with relative standard deviations (RSD%) less than 4%. These results demonstrate the reliability and suitability of the method for accurate quantification of alogliptin in complex biological matrices. To assess the broader applicability of the Tb-CQDs sensor, the method was also employed for the determination of alogliptin in environmental water samples. Salting-out liquid–liquid extraction was utilized to isolate the analyte from river water and tap water matrices. The recovery values obtained were in the range of 99.32–103.79% for the river water samples and 95.10–102.76% for the tap water samples (Table 4). These findings confirm the robustness of the developed method and its ability to accurately quantify alogliptin even in challenging environmental sample types.

Table 4 Recovery analysis of alogliptin in spiked plasma and environmental water samples (river and tap water) using the Tb-CQDs-based fluorescence quenching method

Samples	Spiked ($\mu g\ mL^{-1}$)	Found ($\mu g\ mL^{-1}$)	Recovery (%)	RSD ($n = 3\%$)
Plasma	0.1	0.097	97.07	0.649
	0.5	0.519	103.72	2.403
	1	1.029	102.94	0.274
	1.25	1.218	97.43	3.295
River water	0.1	0.101	101.21	2.517
	0.5	0.519	103.79	2.007
	1	1.033	103.28	3.699
	1.25	1.241	99.32	3.257
Tap water	0.1	0.095	95.10	2.058
	0.5	0.514	102.76	1.276
	1	1.018	101.77	3.066
	1.25	1.21	96.77	3.703

The excellent recovery rates and low variability observed across the plasma, river water, and tap water sample analyses underscore the analytical capabilities of the Tb-CQDs fluorescence technique. The comprehensive validation conducted, including statistical analysis of the recovery data, provides a high degree of confidence in the reliability and accuracy of the alogliptin determination using this nanomaterial-based sensing platform.

3.6. Greenness and blueness assessment

The greenness and blueness assessments conducted on the developed Tb-CQDs fluorescence method provide a comprehensive evaluation of its environmental impact and analytical practicality in comparison to the gold standard HPLC-UV technique[24] (Fig. 6).

Table 3 Comparative statistical analysis of the developed Tb-CQDs fluorescence quenching method and the established HPLC-UV method for determining alogliptin in pharmaceutical formulations

Method	Mean[a]	SD	*t*-Test (2.306)[b]	*P* Value	*F*-Value (6.338)[b]	*P* Value	θ_L[c]	θ_U[c]
Developed method	99.868	1.273	0.218	0.836	5.547	0.126	−1.292	1.562
Reported method	99.733	0.541						

[a] Average of five determinations. [b] The values in parenthesis are tabulated values of "*t*" and "*F*" at ($P = 0.05$). [c] Bias of ±2% is acceptable.

The AGREE assessment, which quantifies the greenness based on the 12 principles of green chemistry, yielded a score of 0.79 for the Tb-CQDs method (Fig. 6A). This is significantly higher than the 0.68 score obtained for the HPLC-UV approach (Fig. 6B), indicating that the Tb-CQDs fluorescence technique is substantially more environmentally friendly. Key factors contributing to the enhanced greenness include the use of non-toxic carbon-based nanomaterials as the sensing platform, the elimination of organic solvents, reduced energy consumption during spectrofluorimetric measurement, and the ability to analyze a higher number of samples per hour. Additionally, the Tb-CQDs method generated less waste compared to the HPLC-UV method.

The blueness assessment using the BAGI tool, which evaluates the analytical practicality in terms of economic and availability factors, resulted in comparable scores between the two methods. The Tb-CQDs approach achieved a BAGI score of 77.5 (Fig. 6C), while the HPLC-UV method scored 80.0 (Fig. 6D). The slightly lower blueness score for the Tb-CQDs method can be attributed to the lack of automation, unlike HPLC-UV systems equipped with autosamplers. However, the higher sample throughput capability of the Tb-CQDs fluorescence method can potentially offset this limitation, leading to the overall comparable blueness profiles. The comprehensive greenness and blueness assessment demonstrates that the developed Tb-CQDs fluorescence method is a more environmentally-friendly and practically viable alternative to the conventional HPLC-UV technique for the determination of alogliptin. The substantial improvement in the greenness score, combined with the comparable blueness, highlights the analytical merits and sustainability advantages of the nanomaterial-based sensing platform.

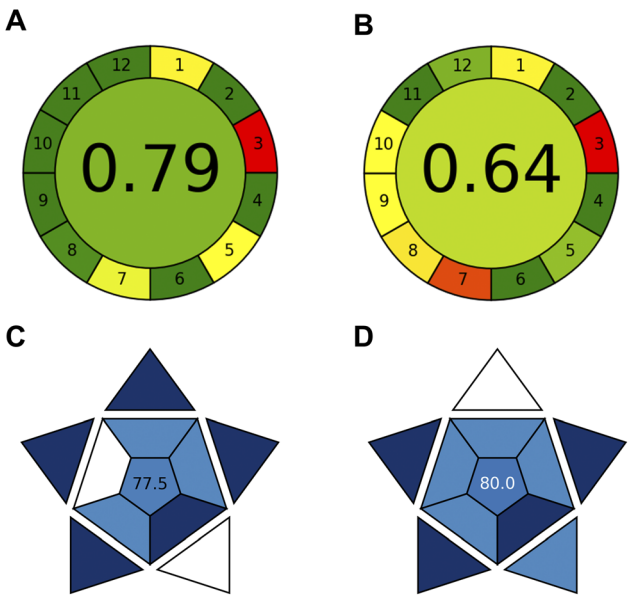

Fig. 6 Greenness and blueness assessments: (A) AGREE score for the developed Tb-CQDs fluorescence method, (B) AGREE score for the HPLC-UV method, (C) BAGI score for the developed Tb-CQDs method, and (D) BAGI score for the HPLC-UV method.

4. Conclusion

In conclusion, the present study established a highly sensitive and selective Tb-CQDs fluorescence-based method for the quantitative determination of the antidiabetic drug alogliptin. The characterization of the Tb-CQDs nanoparticles, mechanistic investigations, and optimization of critical parameters using a Box–Behnken design of experiments provided a robust and reliable analytical platform. Besides, the method was extensively validated according to ICH guidelines, demonstrating excellent linearity in the range of 0.01–1.5 μg mL^{-1}, with a limit of detection as low as 3.20 ng mL^{-1}. The developed method was successfully applied for the analysis of pharmaceutical formulations, spiked human plasma, and environmental water samples, with recovery rates within the acceptable range. Additionally, the greenness and blueness assessments revealed the superior environmental compatibility and comparable analytical practicality of the Tb-CQDs fluorescence technique in comparison to the conventional HPLC-UV approach. The development of this nanomaterial-based sensing platform offers a sustainable, sensitive, and reliable alternative for the routine quantification of alogliptin in various matrices, highlighting its potential for broader application in pharmaceutical and bioanalytical settings.

Future research directions may involve the exploration of other dopant ions or the use of different types of carbon quantum dots to further enhance the sensitivity and selectivity of the fluorescence-based analytical method. Additionally, the using of imprinting polymer techniques such as molecular imprinted polymer can improve the selectivity of the developed sensor. Functionalized Tb-CQDs may also be investigated for their ability to simultaneously detect multiple analytes of interest, expanding the scope of this nanomaterial-based sensing platform. Overall, this study demonstrates the significant potential of Tb-CQDs as a versatile fluorescence probe for the analysis of pharmaceuticals, paving the way for the development of novel, green, and practical analytical methodologies based on advanced fluorescent nanomaterials.

Data availability

The authors confirm that the data supporting the findings of this study are available within the article and its ESI File.†

Conflicts of interest

There are no conflicts of interest to declare.

Acknowledgements

The authors extend their appreciation to Taif University, Saudi Arabia, for supporting this work through project number (TU-DSPP-2024-154).

References

1 F. Belal, M. Mabrouk, S. Hammad, H. Ahmed and A. Barseem, *J. Fluoresc.*, 2024, **34**, 119–138.

2 K. M. Omer, B. Al-Hashimi, S. Mohammadi, A. Salimi, Y. M. Salih, A. Q. Hassan, K. H. H. Aziz and S. J. Mohammad, *J. Mater. Sci.*, 2022, **57**, 14217–14245.
3 E. Petryayeva, W. R. Algar and I. L. Medintz, *Appl. Spectrosc.*, 2013, **67**, 215–252.
4 Z. Zhang, S. Shikha, J. Liu, J. Zhang, Q. Mei and Y. Zhang, *Anal. Chem.*, 2018, **91**, 548–568.
5 M. J. Molaei, *Anal. Methods*, 2020, **12**, 1266–1287.
6 Y. Wang and A. Hu, *J. Mater. Chem. C*, 2014, **2**, 6921–6939.
7 G. Redondo-Fernandez, J. Cigales Canga, A. Soldado, J. Ruiz Encinar and J. M. Costa-Fernandez, *Anal. Chim. Acta*, 2023, **1284**, 341874.
8 C. Verma, S. Dubey, A. Alfantazi and K. Y. Rhee, *J. Ind. Eng. Chem.*, 2024, **133**, 90–111.
9 X. Tian and Z. Fan, *J. Lumin.*, 2022, **244**, 118732.
10 B. B. Chen, Z. X. Liu, H. Y. Zou and C. Z. Huang, *Analyst*, 2016, **141**, 2676–2681.
11 L. Liu, C. Zhang, Y. Yu and F. Chen, *Microchim. Acta*, 2018, **185**, 514.
12 M. Xu, Z. Gao, Q. Zhou, Y. Lin, M. Lu and D. Tang, *Biosens. Bioelectron.*, 2016, **86**, 978–984.
13 S. Gulati, A. Baul, A. Amar, R. Wadhwa, S. Kumar and R. S. Varma, *Nanomaterials*, 2023, **13**, 554.
14 M. J. Molaei, *RSC Adv.*, 2019, **9**, 6460–6481.
15 A. Sharma and J. Das, *J. Nanobiotechnol.*, 2019, **17**, 92.
16 A. S. Alqahtani, F. M. Almutairi, M. M. Aldhafeeri, Y. S. Althobaiti, M. H. Abduljabbar, A. Serag and A. H. Almalki, *Spectrochim. Acta, Part A*, 2025, **327**, 125342.
17 A. H. Almalki, M. H. Abduljabbar, R. M. Alnemari, M. E. Alosaimi, S. I. Alaqel and A. Serag, *Microchem. J.*, 2024, **205**, 111381.
18 K. Wang, Z. Gao, G. Gao, Y. Wo, Y. Wang, G. Shen and D. Cui, *Nanoscale Res. Lett.*, 2013, **8**, 122.
19 M. Havrdova, K. Hola, J. Skopalik, K. Tomankova, M. Petr, K. Cepe, K. Polakova, J. Tucek, A. B. Bourlinos and R. Zboril, *Carbon*, 2016, **99**, 238–248.
20 M. E. Alosaimi, A. H. Almalki, M. H. Abduljabbar, R. M. Alnemari, S. I. Alaqel and A. Serag, *Luminescence*, 2024, **39**, e70060.
21 R. Yin, Y. Xu, X. Wang, L. Yang and D. Zhao, *Molecules*, 2022, **27**, 3055.
22 D. M. Nathan, *JAMA*, 2015, **314**, 1052–1062.
23 B. Lee, L. Shi, D. B. Kassel, T. Asakawa, K. Takeuchi and R. J. Christopher, *Eur. J. Pharmacol.*, 2008, **589**, 306–314.
24 K. Zhang, P. Ma, W. Jing and X. Zhang, *Asian J. Pharm. Sci.*, 2015, **10**, 152–158.
25 H. Naseef, R. Moqadi and M. Qurt, *J. Anal. Methods Chem.*, 2018, **2018**, 1902510.
26 M. A. Attallah, S. Mowaka, E. F. Elkady, M. Fouad and B. Ayoub, *Microchem. J.*, 2019, **148**, 253–261.
27 S. Mowaka, E. F. Elkady, M. M. Elmazar and B. M. Ayoub, *Microchem. J.*, 2017, **130**, 360–365.
28 K. M. Kelani, M. R. Rezk, O. M. Badran and M. R. Elghobashy, *J. Chromatogr. B*, 2019, **1132**, 121803.
29 M. M. Mabrouk, S. F. Hammad, F. R. Mansour and M. M. Amer, *Anal. Chem. Lett.*, 2018, **8**, 368–378.
30 A. R. Derar, N. Ahmed and E. M. Hussien, *BMC Chem.*, 2023, **17**, 79.
31 H. A. Aref, S. F. Hammad, K. M. Darwish and M. S. Elgawish, *Luminescence*, 2020, **35**, 284–291.
32 S. M. Derayea, A. A. Gahlan, M. A. Omar, G. A. Saleh and A. M. Haredy, *Luminescence*, 2020, **35**, 1028–1035.
33 S. M. El-Gizawy, N. N. Atia, D. H. Rushdy and M. F. Ali, *Chem. Pap.*, 2024, 1–12.
34 F. Pena-Pereira, W. Wojnowski and M. Tobiszewski, *Anal. Chem.*, 2020, **92**, 10076–10082.
35 N. Manousi, W. Wojnowski, J. Płotka-Wasylka and V. Samanidou, *Green Chem.*, 2023, **25**, 7598–7604.
36 A. M. Brouwer, *Pure Appl. Chem.*, 2011, **83**, 2213–2228.
37 S. L. C. Ferreira, R. E. Bruns, H. S. Ferreira, G. D. Matos, J. M. David, G. C. Brandão, E. G. P. da Silva, L. A. Portugal, P. S. dos Reis, A. S. Souza and W. N. L. dos Santos, *Anal. Chim. Acta*, 2007, **597**, 179–186.